Nanoscale

Carving the Growing Nanocrystals: Coupling Seed-Mediated Growth with Oxidative Etching

Journal:	*Nanoscale*
Manuscript ID	NR-COM-08-2018-006895.R1
Article Type:	Communication
Date Submitted by the Author:	13-Sep-2018
Complete List of Authors:	Villarreal, Esteban; University of South Carolina, Department of Chemistry and Biochemistry Li, Guangfang; University of South Carolina, Department of Chemistry and Biochemistry Wang, Hui; University of South Carolina, Department of Chemistry and Biochemistry

Journal Name

COMMUNICATION

Carving the Growing Nanocrystals: Coupling Seed-Mediated Growth with Oxidative Etching

Received 00th January 20xx,
Accepted 00th January 20xx

DOI: 10.1039/x0xx00000x

www.rsc.org/

Esteban Villarreal,[a] Guangfang Grace Li,[a] and Hui Wang*[a]

This work presents multiple experimental evidences coherently showing that the versatile structural evolution of Au nanocrystals during seed-mediated growth under the guidance of foreign metal ions and halide-containing surfactants is essentially dictated by the dynamic interplay between oxidative etching and nanocrystal growth. Coupling nanocrystal growth with oxidative etching under kinetically controlled conditions enables *in situ* surface carving of the growing nanocrystals, through which the surface topography of shape-controlled nanocrystals can be deliberately tailored on the nanometer length-scale.

Precise geometry control of nanocrystals through deliberately designed colloidal syntheses forms the keystone for the fine-tuning and rational optimization of the plasmonic and catalytic properties of metallic nanoparticles for widespread applications in nanophotonics,[1] molecular sensing,[2] catalysis,[3] and biomedicine.[4] Fundamentally intriguing and methodologically invaluable to the colloidal nanoscience communities has been the seed-mediated growth of metallic nanocrystals exhibiting thermodynamically unexpected anisotropic geometries.[5-23] The remarkable level of precision and versatility of geometry control realized through seed-mediated growth has been best manifested by the controlled transformations of preformed isotropic Au nanocrystal seeds into an entire family of geometrically distinct anisotropic Au nanostructures, such as nanorods,[5-8] nanoprisms,[9, 10] nanobipyramids,[11] and high-index faceting nanopolyhedra,[12-16] under kinetically controlled conditions synergistically guided by foreign metal ions, most commonly Ag^+, and halide-containing surfactants, typically cetyltrimethylammonium bromide (CTAB) and cetyltrimethylammonium chloride (CTAC).

Although the seed-mediated synthetic protocols developed for various anisotropic nanocrystal geometries appear fairly similar at first glance, variation of any of the synthetic parameters, even to a slight degree, may drastically modify the shapes of the resulting nanocrystals.[13, 17, 18, 23] Such subtlety and versatility of the syntheses are intrinsically tied to the mechanistic complexity of the seed-mediated nanocrystal growth processes. The mechanisms underlying the anisotropic structural evolution of Au nanoparticles have so far been discussed mainly in the context of shape-controlled nanocrystal growth dictated not only by the crystallographic habit of the parental seeds but also more profoundly by the structure-directing additives that regioselectively and dynamically passivate the surfaces of the evolving nanocrystals.[5-23] Several critical aspects regarding the detailed shape-evolving mechanisms, such as the driving force for symmetry-breaking, the structural dynamics at the evolving particle/solution interfaces, and the exact roles of Ag^+ foreign cations and the halide counter ions of the surfactants, however, have long been intensively debated and still remain ambiguous.[6, 17, 18, 24-28] According to the shape-defining rules proposed by Mirkin and coworkers,[17] the seed-mediated shape evolution of multifaceted Au nanocrystals is essentially dictated by the underpotential deposition (UPD) of Ag adatoms on Au nanocrystal surfaces, which selectively stabilizes certain types of crystallographic facets. The halide anions, on the other hand, regulate the Au deposition kinetics by forming complexes with ionic gold species and further modulate the coverage and stability of the Ag UPD adlayer through surface capping. Previous experimental observations and computational results suggest that a strong synergy exists between the Ag UPD layer and the surface-capping halide anions.[6, 17, 18, 25] While the above-mentioned shape-defining rules seem broadly applicable when interpreting ample examples in the literature, our observations reported here strongly indicate that the growth of Au nanocrystals is entangled with oxidative etching under the Ag^+- and CTAC-coguided seed-mediated growth conditions, and thus is mechanistically even more complicated than people typically thought. To fully decipher the complex mechanisms underpinning the intriguing structural evolution of nanocrystals during seed-mediated growth, oxidative etching must be added as a pivotal missing piece to the puzzle.

We employed CTAC-capped Au colloids (~ 4 nm in diameter, see Figure S1 in Electronic Supplementary Information†) as the seeds to guide the shape evolution of Au nanocrystals at room temperature under ambient air in aqueous growth solutions containing $HAuCl_4$ as

[a] Department of Chemistry and Biochemistry, University of South Carolina, Columbia, South Carolina 29208, United States. Email: wang344@mailbox.sc.edu.
†Electronic Supplementary Information (ESI) available.
See DOI: 10.1039/x0xx00000x

the ionic gold precursor, CTAC as a surface-capping surfactant, ascorbic acid (AA) as a mild reducing agent, $AgNO_3$ as the source of Ag^+ foreign ions, and HCl as a pH regulator. In the absence of seeds, $AuCl_4^-$ was first reduced by AA to form $AuCl_2^-$, which was further reduced to metallic Au upon the addition of seeds to the growth solution.[6, 13, 18] The rate of the seed-mediated Au reduction was pH dependent, increasing with the pH of the growth solution.[6, 17, 18, 28] On the other hand, the O_2 dissolved in the growth solution was capable of mildly oxidizing the Au atoms on the surfaces of the growing nanocrystals to form $AuCl_2^-$ with the aid of Cl^- as the complexing agent through the following reaction:[29]

$$4Au + O_2 + 8Cl^- + 4H^+ \rightarrow 4AuCl_2^- + 2H_2O$$

This etching process could be kinetically boosted by simply decreasing the pH of the growth solution without introducing any additional strong oxidants. As demonstrated by Wang, Stucky, and coworkers,[29] preformed single-crystalline Au nanorods underwent a shortening process driven by selective etching along their longitudinal axis in the presence of dissolved O_2 and CTAC or CTAB in an acidic environment. Xia and coworkers [30-32] also employed halide anions and O_2 in polyol solvents as mild etchant pairs to carve the surfaces of metallic nanocrystals in a site-selective manner. Here, we used HCl as a unique synthetic knob to tune the relative rates of oxidative etching *vs.* nanocrystal growth, through which we were able to fine-tailor the surface topography of nanocrystals adopting several primary geometries, such as quasi-spheres, cubes, and cuboctahedra, by controllably carving the surfaces of the growing nanocrystals *in situ*.

Increase of HCl concentration, C_{HCl}, in the growth solution sped up the oxidative etching while simultaneously slowing down the nanocrystal growth. We systematically varied the C_{HCl} in the range of 0-25 mM while fixing the concentrations of $HAuCl_4$, $AgNO_3$, CTAC, and AA at 500 μM, 50 μM, 100 mM, and 1.2 mM, respectively. After the reactions proceeded for 16 h, we kinetically trapped the resulting nanostructures by separating them from their native growth solutions through centrifugation followed by redispersion in water. As revealed by the scanning electron microscopy (SEM) images in Figure 1A-1G, alteration of C_{HCl} markedly modified the shapes and surface topography of the resulting nanocrystals. At C_{HCl} below 3 mM, the isotropic seeds evolved into surface-roughened quasi-spherical nanoparticles (SRQSNPs, Figure 1A-1B) as a consequence of mild etching of fast-growing nanocrystals. In the intermediate C_{HCl} regime (5-15 mM), the etching effects became more pronounced, resulting in surface-textured concave nanocubes (STCNCs, Figure 1C-1E), which were derived from nanocubes through selective corrosion of the {100} side facets coupled with preferential Au deposition on the edges. When C_{HCl} was further increased to above 15 mM, oxidative etching became even faster while nanocrystal growth was further slowed down, leading to the formation of excavated cuboctahedral nanoparticles (ECONPs, Figure 1F-1G), a geometry derived from a nano-cuboctahedron by creating indentation on the {100} facets while retaining the {111} facets at the truncated corners.

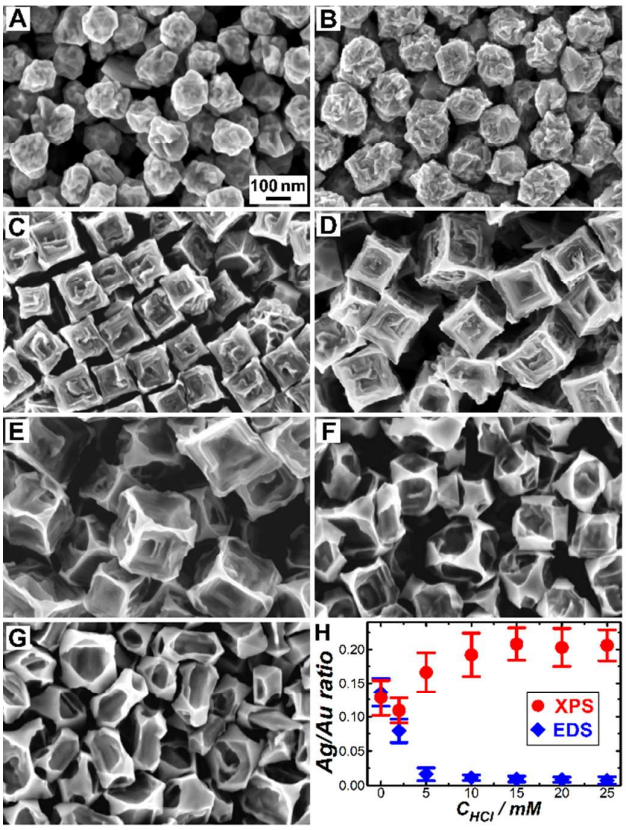

Figure 1. SEM images of nanoparticles synthesized after 16 h in growth solutions containing 100 mM CTAC, 50 μM $AgNO_3$, 500 μM $HAuCl_4$, and 1.2 mM AA at various C_{HCl}: (A) 0, (B) 2, (C) 5, (D) 10, (E) 15, (F) 20, (G) 25 mM. All SEM images share the same scale bar in panel A. (H) Ag/Au atomic ratios quantified by XPS (red circles) and EDS (blue rhombi) for nanoparticles synthesized at various C_{HCl}. The error bars represent the standard deviations obtained from 3 samples synthesized under identical conditions.

We used X-ray photoelectron spectroscopy (XPS) and energy dispersive spectroscopy (EDS) to characterize the surface and bulk compositions of the nanoparticles, respectively. In comparison to the XPS features of bulk Ag and Au foils, the Ag 3d peaks of the nanoparticle samples significantly downshifted by ~ 0.4 eV, while the Au 4f peaks slightly upshifted by less than ~ 0.05 eV (Figure S2†), indicating the atomic intermix of Ag with Au either on the surfaces or in the sub-surface regions of the nanocrystals.[13, 28] While Ag signals were clearly resolvable by XPS on all samples, Ag became almost undetectable by EDS on the samples synthesized at C_{HCl} above 5 mM (Figure S3†). In Figure 1H, we compared the surface and bulk Ag/Au atomic ratios quantified by XPS and EDS, respectively, for the nanoparticle samples obtained at various C_{HCl}. At C_{HCl} below 5 mM, EDS and XPS gave nominally the same Ag/Au atomic ratios (in the range of ~0.08-0.15), indicating that the SRQSNPs were essentially composed of Au-Ag alloys rather than phase-segregated core-shell heterostructures. Such alloy structure was further confirmed by EDS elemental mapping (Figure S4†). For the nanoparticles synthesized at C_{HCl} above 5 mM, the EDS signals of Ag became vanishingly weak while the surface Ag/Au atomic

ratios quantified by XPS remained in the range of 0.15-0.22, strongly indicating that Ag existed as a UPD atomic adlayer on the nanocrystal surfaces. The structural transition from Au-Ag alloy nanocrystals to Ag adatom-capped Au nanocrystals as C_{HCl} increased could be well interpreted as a consequence of pathway switch from Au-Ag codeposition to Ag UPD-mediated Au deposition. Detailed mechanisms underpinning this pathway switch were recently elucidated by our group using shape-controlled nanorod overgrowth as a prototypical system.[28]

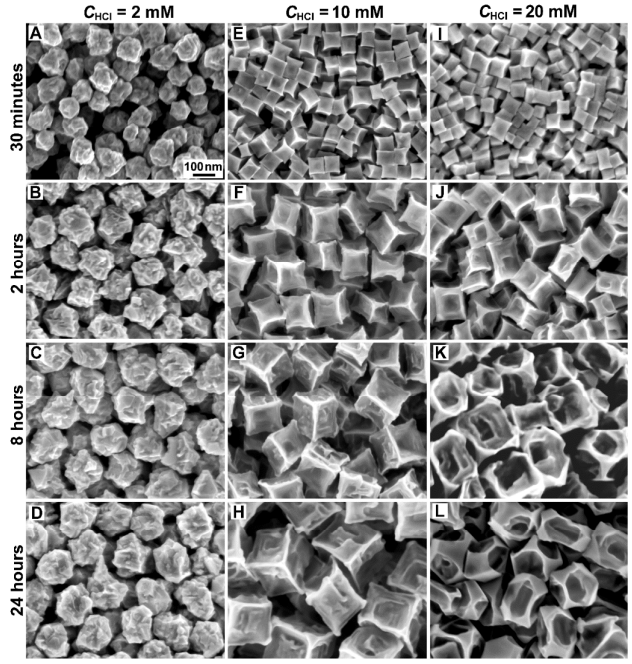

Figure 2. SEM images of nanoparticles synthesized in growth solutions containing 50 μM $AgNO_3$, 500 μM $HAuCl_4$, 100 mM CTAC, and 1.2 mM AA at different C_{HCl} after various reaction times: (A) 2 mM HCl, 0.5 h; (B) 2 mM HCl, 2 h; (C) 2 mM HCl, 8 h; (D) 2 mM HCl, 24 h; (E) 10 mM HCl, 0.5 h; (F) 10 mM HCl, 2 h; (G) 10 mM HCl, 8 h; (H) 10 mM HCl, 24 h; (I) 20 mM HCl, 0.5 h; (J) 20 mM HCl, 2 h; (K) 20 mM HCl, 8 h; (L) 20 mM HCl, 24 h. All SEM images share the same scale bar in panel A.

To gain further insights into the temporal evolution of nanoparticle morphologies, we kinetically trapped the nanocrystals at various stages during the reactions. At the early stages of the reactions, the growth of nanocrystals was much faster than oxidative etching. As the reactions further proceeded, the nanocrystal growth became progressively slower due to the continuous consumption of the $AuCl_2^-$, eventually approaching an equilibrium when the growth and etching rates became equivalent. At C_{HCl} of 2 mM, the seeds rapidly evolved into SRQSNPs and the nanoscale surface textures were well-preserved throughout the entire growth/etching process (Figure 2A-2D). The particle sizes rapidly increased before reaching a plateau after ~ 2 h (Figure S5A†). When C_{HCl} was raised to 10 mM, the seeds first transformed into concave nanocubes enclosed by indented side facets, followed by nanoscale texturing of the nanocrystal surfaces (Figure 2E-2H). As the reactions proceeded, the degree of surface indentation increased, accompanied by progressive increase of the edge-lengths of STCNCs (Figure S5B†). Concave nanocubes were also found to be the early-stage intermediates during the reactions at C_{HCl} of 20 mM. Under this condition, fast etching of the slowly-growing nanocrystals led to not only the indentation of the side facets but also preferential oxidation of the undercoordinated surface atoms at the corners of the cube-shaped nanocrystals (Figure 2I-2L). Therefore, well-defined, thermodynamically favored {111} facets gradually developed at the truncated corners when the nanocrystal growth became much slower than etching at the late stages of the reactions.

We tracked the temporal evolution of the nanocrystal compositions *ex situ* using XPS and EDS (Figure S6†). The Ag/Au stoichiometric ratios of the alloy SRQSNPs remained essentially unchanged during seed-mediated growth, suggesting that Au and Ag were deposited at a constant relative rate. When the nanocrystal shape evolution was dominated by Ag-UPD, the Ag adatom coverage on the nanoparticle surfaces (quantified by XPS) increased over time till reaching equilibria, while the Ag signals remained almost undetectable by EDS throughout the entire processes. We also used inductively coupled plasma mass spectrometry (ICP-MS) to quantify the total amounts of gold and silver remaining in the supernatant at various reaction times after separating the nanocrystals from the growth solutions (Figure S7†). At C_{HCl} of 2 mM, the total amounts of both gold and silver in the growth solutions progressively decreased until reaching the deposition/etching equilibrium as a consequence of seed-mediated Au-Ag co-deposition. When Ag UPD-mediated Au deposition occurred at C_{HCl} of 10 and 20 mM, the gold precursors were gradually consumed while the total amount of silver species in the growth solutions remained almost unchanged. The structural evolution of the nanocrystals was further monitored *in situ* using optical extinction spectroscopy without separating the nanocrystals from their growth solutions. As shown in Figure S8†, increase of particle sizes, development of surface concavity, and introduction of surface textures all led to spectral redshift and broadening of the plasmon resonance peaks, whereas the plasmon resonances blue-shifted upon corner truncation. The temporal evolution of the extinction spectroscopic features was discussed in greater detail in the Electronic Supplementary Information.

Increasing AA concentration, C_{AA}, while keeping the other synthetic parameters unchanged allowed us to accelerate the nanocrystal growth without modifying the etching rate. At C_{HCl} of 2 mM, the surface roughness of the nanocrystals could be tailored by varying the relative growth and etching rates, achieving the highest degree of surface texturing within a C_{AA} window of 1-2 mM (Figure S9A-S9C†). At C_{HCl} of 20 mM, structural transitions from ECONPs to STCNCs and eventually to SRQSNPs were observed as C_{AA} progressively increased from 1 to 5 mM (Figure S9D-S9F†) due to acceleration of nanocrystal growth. The oxidative etching could also be kinetically modulated without changing the nanocrystal growth rate by simply varying the concentration of O_2 dissolved in the growth solution. Saturating the growth solution with O_2 resulted in loss of nanoscale surface textures and decrease of particle sizes (Figure S10A-S10C†) due to enhanced oxidative etching. When the growth solution was purged with N_2 to eliminate the dissolved O_2, the oxidative etching was effectively suppressed and the surface-roughened quasi-spherical morphology was preserved over a broad

C_{HCl} range even up to 20 mM (Figure S10D-S10F†). Interestingly, both the surface and bulk Ag/Au atomic ratios of the nanocrystals appeared almost independent of the concentration of O_2 dissolved in the growth solution (Figure S11†), indicating that the nanocrystal compositions were essentially determined by the relative Ag and Au deposition rates rather than the relative rates of etching *vs.* growth.

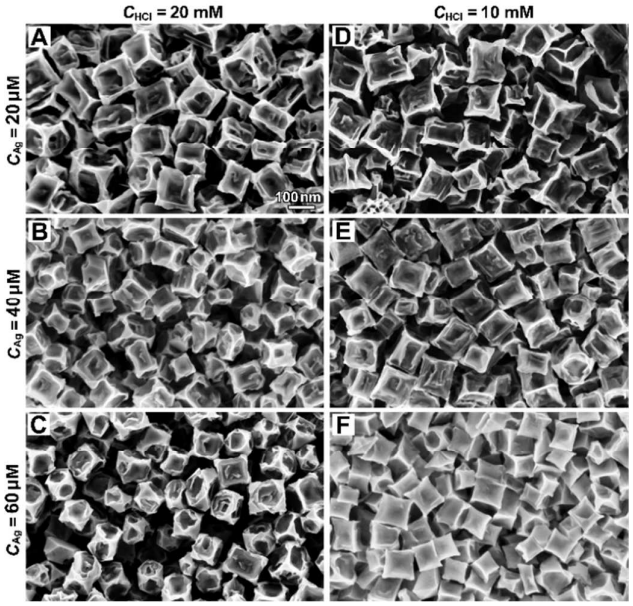

Figure 3. SEM images of nanoparticles synthesized after 16 h in growth solutions containing 100 mM CTAC, 500 μM $HAuCl_4$, 1.2 mM AA, and various concentrations of HCl and $AgNO_3$: (A) 20 mM HCl, 20 μM $AgNO_3$; (B) 20 mM HCl, 40 μM $AgNO_3$; (C) 20 mM HCl, 60 μM $AgNO_3$; (D) 10 mM HCl, 20 μM $AgNO_3$; (E) 10 mM HCl, 40 μM $AgNO_3$; (F) 10 mM HCl, 60 μM $AgNO_3$. All SEM images share the same scale bar in panel A.

While the effects of Ag^+ foreign ions on the seed-mediated growth of Au nanocrystals of various shapes have been well-documented in the literature,[6, 17, 18, 24-28] we found that the Ag^+ foreign ions also played crucial roles in guiding the regioselective etching of nanocrystal surfaces. At C_{HCl} of 20 mM, the degree of corner truncation increased while the surface concavity decreased as the $AgNO_3$ concentration, C_{Ag}, progressively increased in the range of 20-60 μM (Figure 3A-C). Increase of C_{Ag} resulted in higher coverage of Ag UPD adatoms on the side facets of a cube-shaped nanoparticle, effectively slowing down the surface indentation process. However, the undercoordinated surface atoms located around the corners of a cube-shaped nanocrystal still remained prone to etching. Preferential etching of the corners with respect to the side facets, coupled with preferential Au deposition on the edges led to the formation of ECONPs. When C_{HCl} decreased to 10 mM, the surfaces of the STCNCs became less concave and increasingly smoother while the sharp corners were still preserved as the surface coverage of Ag adatoms increased (Figure 3D-F), primarily due to slower etching of the corners and side facets. Removal of $AgNO_3$ from the growth solution resulted in faster oxidative etching, drastically modifying the structure-transforming process. Under the Ag-free conditions, the Au seeds evolved into SRQSNPs at low C_{HCl}. As C_{HCl} increased, the feature sizes of surface textures increased and well-defined crystallographic facets started to develop on the nanocrystal surfaces, resulting in blue-shift of the plasmon resonance in the extinction spectra (Figure S12†).

We further compared the post-synthetic etching of preformed Au concave nanocubes and Au-Ag alloy SRQSNPs in etching solutions containing 100 mM CTAC and 10 mM HCl, either with or without 50 μM $AgNO_3$. Apparently, the etching proceeded significantly faster in the Ag-free environment, resulting in more drastic decrease of the particles sizes (Figure S13†). The Au SRQSNPs synthesized in the absence of Ag^+ foreign ions appeared even more vulnerable to oxidative etching than the Au-Ag alloy SRQSNPs, completely losing their surface textures after exposure to an etching solution containing 100 mM CTAC and 10 mM HCl under ambient air for 16 h (Figure S14†). Therefore, the nanoscale surface textures were essentially a unique structural feature resulting from *in situ* mild surface etching of nanocrystals growing at appropriate rates.

In summary, multiple observations coherently indicate that oxidative etching interplays with nanocrystal growth under kinetically controlled conditions to guide the versatile structural evolution of Au nanocrystals during seed-mediated growth. This work provides important implications that may help us more comprehensively understand the seed-mediated growth of complex nanostructures when revisiting previously reported examples in the literature. Seed-mediated growth of various anisotropic nanostructures, such as nanorods and nanoprisms, may all involve site-selective etching of the growing nanocrystals, especially at the early stages when the symmetry of the isotropic seeds gets broken.[6, 9, 10, 26, 27] Another interesting example is the overgrowth of concave nanocube seeds into hollow Au nano-octahedra in a growth solution containing AA and HCl at a significantly higher $AgNO_3/HAuCl_4$ ratio of 1:1.[33] While the formation of the hollow octahedral nanoparticles was previously interpreted as the consequence of Ag UPD-stabilized {111} facet growth at the corners of the concave nanocube seeds, it is highly likely that oxidative etching is also responsible for the growth of the intraparticle cavities. Here we have demonstrated that the nanoscale surface topography of shape-controlled nanocrystals can be fine-tailored through deliberate kinetic control of oxidative etching with respect to nanocrystal growth. Introduction of nanoscale surface textures to sub-wavelength metallic nanoparticles greatly expands the plasmonic tuning range and enhances the local electric fields exploitable for plasmon-enhanced spectroscopies.[34] In addition, surface-textured metallic nanoparticles may serve as an ideal model system for us to study how nanoscale surface texturing affects the light scattering properties of roughened nanostructures naturally existing in environmental and biological systems,[35] such as atmospheric dust particles and subcellular organelles. Furthermore, the surface-textured nanocrystals are enclosed by highly abundant undercoordinated surface atoms, which may serve as the active sites for heterogeneous catalysis.[36] Combination of desired plasmonic and catalytic properties on the same metallic nanocrystals further enables us to monitor intriguing catalytic molecular transformations in real time using plasmon-enhanced Raman scattering as a time-resolving and molecular finger-printing spectroscopic tool.[37-39] As exemplified by this work and several previous publications,[30, 40-42] judiciously coupling nanocrystal

growth with oxidative etching, galvanic replacement, or other redox processes enables controlled synthesis of structurally sophisticated nanocrystals exhibiting exotic geometries and fine-tailored surface topography, greatly enhancing our capabilities to further fine-optimize the optical and catalytic properties of nanoparticles for specific applications.

Conflicts of interest

There are no conflicts to declare.

Acknowledgment

This work was supported by National Science Foundation through an EPSCoR RII Track-I Award (OIA-1655740). E.V. was partially supported by a GAANN Fellowship provided by the Department of Education through GAANN Award P200A120075.

Notes and references

1. A. Moreau, C. Ciraci, J. J. Mock, R. T. Hill, Q. Wang, B. J. Wiley, A. Chilkoti and D. R. Smith, *Nature*, 2012, **492**, 86-89.
2. J. N. Anker, W. P. Hall, O. Lyandres, N. C. Shah, J. Zhao and R. P. Van Duyne, *Nat. Mater.*, 2008, **7**, 442-453.
3. C. Chen, Y. J. Kang, Z. Y. Huo, Z. W. Zhu, W. Y. Huang, H. L. L. Xin, J. D. Snyder, D. G. Li, J. A. Herron, M. Mavrikakis, M. F. Chi, K. L. More, Y. D. Li, N. M. Markovic, G. A. Somorjai, P. D. Yang and V. R. Stamenkovic, *Science*, 2014, **343**, 1339-1343.
4. P. K. Jain, X. H. Huang, I. H. El-Sayed and M. A. El-Sayed, *Acc. Chem. Res.*, 2008, **41**, 1578-1586.
5. B. Nikoobakht and M. A. El-Sayed, *Chem. Mater.*, 2003, **15**, 1957-1962.
6. S. E. Lohse and C. J. Murphy, *Chem. Mater.*, 2013, **25**, 1250-1261.
7. J. Perez-Juste, I. Pastoriza-Santos, L. M. Liz-Marzan and P. Mulvaney, *Coord. Chem. Rev.*, 2005, **249**, 1870-1901.
8. L. Scarabelli, A. Sanchez-Iglesias, J. Perez-Juste and L. M. Liz-Marzan, *J. Phys. Chem. Lett.*, 2015, **6**, 4270-4279.
9. J. E. Millstone, S. J. Hurst, G. S. Metraux, J. I. Cutler and C. A. Mirkin, *Small*, 2009, **5**, 646-664.
10. L. Scarabelli, M. Coronado-Puchau, J. J. Giner-Casares, J. Langer and L. M. Liz-Marzan, *ACS Nano*, 2014, **8**, 5833-5842.
11. M. Z. Liu and P. Guyot-Sionnest, *J. Phys. Chem. B*, 2005, **109**, 22192-22200.
12. J. A. Zhang, M. R. Langille, M. L. Personick, K. Zhang, S. Y. Li and C. A. Mirkin, *J. Am. Chem. Soc.*, 2010, **132**, 14012-14014.
13. M. L. Personick, M. R. Langille, J. Zhang and C. A. Mirkin, *Nano Lett.*, 2011, **11**, 3394-3398.
14. Q. Zhang, N. Large and H. Wang, *ACS Appl. Mater. Interfaces*, 2014, **6**, 17255-17267.
15. T. Ming, W. Feng, Q. Tang, F. Wang, L. D. Sun, J. F. Wang and C. H. Yan, *J. Am. Chem. Soc.*, 2009, **131**, 16350-16351.
16. T. T. Tran and X. M. Lu, *J. Phys. Chem. C*, 2011, **115**, 3638-3645.
17. M. R. Langille, M. L. Personick, J. Zhang and C. A. Mirkin, *J. Am. Chem. Soc.*, 2012, **134**, 14542-14554.
18. S. E. Lohse, N. D. Burrows, L. Scarabelli, L. M. Liz-Marzan and C. J. Murphy, *Chem. Mater.*, 2014, **26**, 34-43.
19. Y. N. Xia, X. H. Xia and H. C. Peng, *J. Am. Chem. Soc.*, 2015, **137**, 7947-7966.
20. C. J. DeSantis, A. A. Peverly, D. G. Peters and S. E. Skrabalak, *Nano Lett.*, 2011, **11**, 2164-2168.
21. R. G. Weiner, M. R. Kunz and S. E. Skrabalak, *Acc. Chem. Res.*, 2015, **48**, 2688-2695.
22. W. X. Niu, W. Q. Zhang, S. Firdoz and X. M. Lu, *J. Am. Chem. Soc.*, 2014, **136**, 3010-3012.
23. T. K. Sau and C. J. Murphy, *J. Am. Chem. Soc.*, 2004, **126**, 8648-8649.
24. J. A. Edgar, A. M. McDonagh and M. B. Cortie, *ACS Nano*, 2012, **6**, 1116-1125.
25. N. Almora-Barrios, G. Novell-Leruth, P. Whiting, L. M. Liz-Marzan and N. Lopez, *Nano Lett.*, 2014, **14**, 871-875.
26. M. J. Walsh, S. J. Barrow, W. M. Tong, A. M. Funston and J. Etheridge, *ACS Nano*, 2015, **9**, 715-724.
27. M. J. Walsh, W. M. Tong, H. Katz-Boon, P. Mulvaney, J. Etheridge and A. M. Funston, *Acc. Chem. Res.*, 2017, **50**, 2925-2935.
28. Q. Zhang, H. Jing, G. G. Li, Y. Lin, D. A. Blom and H. Wang, *Chem. Mater.*, 2016, **28**, 2728-2741.
29. C. K. Tsung, X. S. Kou, Q. H. Shi, J. P. Zhang, M. H. Yeung, J. F. Wang and G. D. Stucky, *J. Am. Chem. Soc.*, 2006, **128**, 5352-5353.
30. Y. Q. Zheng, J. Zeng, A. Ruditskiy, M. C. Liu and Y. N. Xia, *Chem. Mater.*, 2014, **26**, 22-33.
31. M. C. Liu, Y. Q. Zheng, L. Zhang, L. J. Guo and Y. N. Xia, *J. Am. Chem. Soc.*, 2013, **135**, 11752-11755.
32. A. Ruditsicy, M. Vara, H. Huang and Y. N. Xia, *Chem. Mater.*, 2017, **29**, 5394-5400.
33. M. R. Langille, M. L. Personick, J. Zhang and C. A. Mirkin, *J. Am. Chem. Soc.*, 2011, **133**, 10414-10417.
34. Q. F. Zhang, N. Large, P. Nordlander and H. Wang, *J. Phys. Chem. Lett.*, 2014, **5**, 370-374.
35. H. Wang, K. Fu, R. A. Drezek and N. J. Halas, *Appl. Phys. B-Lasers Opt.*, 2006, **84**, 191-195.
36. Q. F. Zhang, D. A. Blom and H. Wang, *Chem. Mater.*, 2014, **26**, 5131-5142.
37. Q. F. Zhang, L. L. Han, H. Jing, D. A. Blom, Y. Lin, H. L. L. Xing and H. Wang, *ACS Nano*, 2016, **10**, 2960-2974.
38. Q. F. Zhang, Y. D. Zhou, E. Villarreal, Y. Lin, S. L. Zou and H. Wang, *Nano Lett.*, 2015, **15**, 4161-4169.
39. J. W. Zhang, S. A. Winget, Y. R. Wu, D. Su, X. J. Sun, Z. X. Xie and D. Qin, *ACS Nano*, 2016, **10**, 2607-2616.
40. Z. N. Wang, H. Wang, Z. R. Zhang, G. Yang, T. O. He, Y. D. Yin and M. S. Jin, *ACS Nano*, 2017, **11**, 163-170.
41. L. Polavarapu, D. Zanaga, T. Altantzis, S. Rodal-Cedeira, I. Pastoriza-Santos, J. Perez-Juste, S. Bals and L. M. Liz-Marzan, *J. Am. Chem. Soc.*, 2016, **138**, 11453-11456.
42. L. Chen, F. Ji, Y. Xu, L. He, Y. F. Mi, F. Bao, B. Q. Sun, X. H. Zhang and Q. Zhang, *Nano Lett.*, 2014, **14**, 7201-7206.

Table of Content Entry:

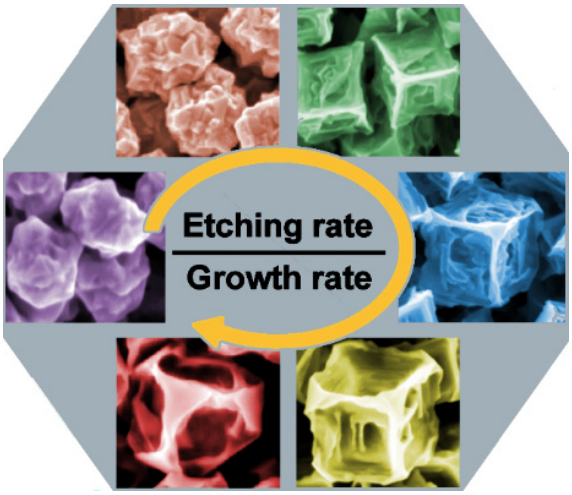

The dynamic interplay between nanocrystal growth and oxidative etching dictates the versatile structural evolution of Au nanocrystals during seed-mediated growth.